Hindawi
Mathematical Problems in Engineering
Volume 2024, Article ID 4418858, 12 pages
https://doi.org/10.1155/2024/4418858

Research Article

Real-Time Frequency-Tracking Method Based on Interpolated Kalman Filter Using Vibration and Surface Noise

Chengcheng Li,[1,2] **Yuan Wan**,[1] **Pingheng Pan**,[1] **Bian Hu**,[1] **and Junhao Zhang**[3]

[1]*Hunan Wuling Power Technology Co., Ltd., Hunan 410029, China*
[2]*College of Electrical and Information Engineering, Hunan University, Hunan 410082, China*
[3]*Changsha Social Laboratory of Artificial Intelligence, Hunan University of Technology and Business, Hunan 410205, China*

Correspondence should be addressed to Junhao Zhang; luoyzjh@163.com

Received 25 October 2023; Revised 7 December 2023; Accepted 16 January 2024; Published 30 January 2024

Academic Editor: Yu-Ling He

The variation of frequency is a significant indicator of the operation status of rotating machinery. Generally, the frequency is extracted and tracked in real-time based on the vibration signal produced by the rotating machinery. However, various interferences generated from contact sampling and transmitting result in difficulty in obtaining the frequency correctly in real-time from the vibration. To solve this problem, this paper presents an interpolated Kalman filter (IKF) based on the vibration and surface noise signals for real-time frequency tracking. First, the cross-correlation operation is performed on the vibration and surface noise signals sampled synchronously to enhance the energy concentration. After that, a frequency search procedure is carried out to calculate the input of the tracking task. Finally, an IKF-based frequency lock procedure is applied to eliminate the interferences and track the frequency in real time. Besides, a correction procedure is added to prevent the measurement process from tracking the frequency incorrectly. The performance of the proposed method is verified by the experiments based on an ARM-based test bench using standard signals and actual test signals.

1. Introduction

Rotating machinery, such as generators, motors, and engines, plays a crucial role in modern industry and life [1–3]. For example, hydraulic generators, thermal generators, wind turbines, etc., convert various energy sources into the electrical power, while motors and engines convert electrical and chemical power into the mechanical energy, respectively, to drive various devices [4, 5]. However, malfunction is unavoidable in the operation of rotating machinery, and the failure of rotating machinery not only causes damage to these devices themselves but also causes large economic losses and casualties [6, 7]. Meanwhile, with the continuous development of technology, higher reliability, stability, and safety of rotating machinery are required for high-quality production and life. Thus, it is of great significance to monitor the running status of rotating machinery in real time to predict and diagnose potential faults to ensure normal operation [8–10].

The fault diagnosis of rotating machinery usually takes the time-domain, frequency-domain, and time–frequency domain features extracted from the sampled device-produced signals first, and then a classifier is adopted to achieve the classification of faults occurred based on the features [11–13]. In [14], a flexible time–frequency analysis method is proposed to isolate and identify multiple faults occurring in the different components of rolling bearings. The authors in [15] proposed a residual generator based on Kalman filter (KF) to detect the faults in a linear drive system affected by system noise. In [16], a decision tree and deep neural network combined method is proposed to detect and classify the faults in wind turbine generators through the analysis of features in the stator current signals. Literature by Li et al. [17] uses the back propagation neural network and improved genetic algorithm to diagnose the complex fault of marine generators.

Generally, the features are extracted from the surface vibration signals sourced by the rotation moves [18, 19], because lots of research have confirmed that there are differences in the vibration signals of faulty and nonfaulty rotating machinery [20, 21]. These differences are specifically reflected in vibration displacement, speed, frequency, and other aspects [22, 23].

In [24], a variation Hilbert–Huang transform is proposed to extract the time–frequency domain features of the vibration signal for weak bearing fault diagnosis. Among the features, frequency is the most important one as it can accurately reflect the running state of rotating machinery [25]. For example, the frequency of the engine vibration is a significant indicator for the status assessment of a vehicle. Many techniques have been applied to extract the frequency, e.g., wavelet transform (WT) [26], Hilbert–Huang transform [27], empirical mode decomposition [28], variational mode decomposition [29], FFT (fast Fourier transform), short-term Fourier transform (STFT) [30], etc. Among these, the FFT, which is a fast version of the DFT (discrete Fourier transform), is widely used to deal with the vibration signal to estimate the frequency in real time in virtue of its low-computational burden and high efficiency [31]. In [32], a rectangular-based DFT for frequency estimator is proposed to track the power system frequency in a short observation window. To acquire the chatter frequency of machining processes, a high anti-noise frequency estimator based on DFT using zero padding technique is given in [33], which is named SDFT. Unlike the power signals that can be sampled directly, the vibration signal of rotating machinery is acquired contact generally, which will be affected by various interferences, and thus decreases the accuracy of frequency tracking. Thereby, the surface noise is taken as an auxiliary for fault diagnosis, since the surface noise is a production of the vibration [34, 35]. For instance, in [36], the vibration noise of the transformer electromagnetic is analyzed and taken advantage of, to give assistance to the main frequency components analysis. The author in [37] made use of vibration and noise to detect and monitor the cavitation in the kinetic pumps.

However, the mentioned methods suffer from poor accuracy and heavy computational burden, which may not be suitable for real-time field frequency tracking under the complex working conditions. To this end, an interpolated Kalman filter (IKF) based on windowed FFT is proposed in this paper to track the frequency of rotating machinery efficiently and accurately. By using the KF, the proposed method can track the abrupt changes in frequency and filter out the strong interferences that exceed the main component of the vibration signal. Together with the windowed FFT, fine frequency estimation can be acquired with a lower computation burden. Results of the practical applications are provided to show that the proposed method can improve the accuracy of frequency tracking significantly.

The contribution of this paper can be twofolded: (1) A combined method using vibration and surface noise signals for real-time frequency tracking of the rotating machinery working under complex conditions is proposed; (2) A low-cost ARM-based test bench is set up for real-time frequency-tracking task using the vibration and surface noise signals.

The remainder of this paper is organized as follows: first, the principle of measurement based on vibration signal and the test bench setup is introduced, followed by the concept of the improved method, and the calculation formulas including the principles of KF are presented. Then, practical experiments that can evaluate the performance of frequency-tracking method and the test results are shown. Finally, the conclusion is drawn.

2. Principle of Measurement

Generally, there is a direct relationship between the revolutions per minute (RPM) of the rotating machinery and the fundamental frequency (FF) of the vibrations. Therefore, the vibration frequency of the motor can be used to reflect the running state of the motor and the stability of the mechanical structure. For the generators, e.g., hydroelectric generator, thermal generator, wind turbine, etc., the vibration frequency of the generator is proportional to the RPM, i.e., the faster the speed is, the higher the vibration frequency is. The relationship between the RPM and FF f_0 of generators can be presented as follows:

$$\mathrm{RPM} = \frac{120 \cdot f_0}{\alpha}, \tag{1}$$

where α means the pole logarithm of a generator. While for the engine, the mathematical relationship between RPM and FF of vibration signal could be represent as follows:

$$\mathrm{RPM} = 60 \cdot (f_0/\omega) \cdot (\lambda/2), \tag{2}$$

where ω is the number of cylinders and λ is the number of strokes. It can be known that once ω and λ are fixed, the ratio between RPM and FF settles down to be a constant. Then, the problem of RPM can turn into the FF estimation of the vibration signal.

Normally, the sampled vibration signal can be expressed as follows:

$$x(n) = \sum_{i=1}^{I} [A_i(n)\sin(2\pi f_i(n)n + \varphi_i(n))] + \xi(n), \tag{3}$$

where $i = 1, 2, 3, \ldots, I$, I is the number of frequency components; A_i, f_i, and φ_i are the amplitude, frequency, and phase angle of the i-th harmonic, respectively, which are all time-varying variables in the actual; ξ is the interference component produced by the structure of rotating equipment, and transmission, as well as abnormality.

Generally, the amplitude of FF is the maxima in the spectrum and the total error ξ, as well as the harmonics, can be neglected for the FF measurement. To clearly demonstrate this, Figure 1 shows the spectrum of the normal vibration signal acquired from a standard vibration exciter.

From Figure 1, it can be seen that there is only one peak in the spectrum, which is easy to determine where the FF is. Accordingly, the flowchart for tracking the frequency using the vibration signal is given in Figure 2, which can be represented as follows:

(1) Acquire the vibration signal using transducers;
(2) Filter the high-frequency interference of the vibration signal with the condition circuit;
(3) Acquire the discrete vibration signal with ADC;
(4) Filter the discrete vibration signal using a digital filter;

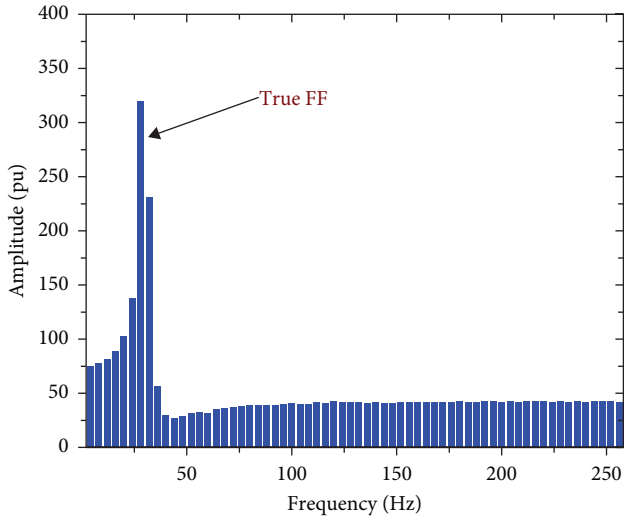

Figure 1: Spectrum of the normal vibration signal.

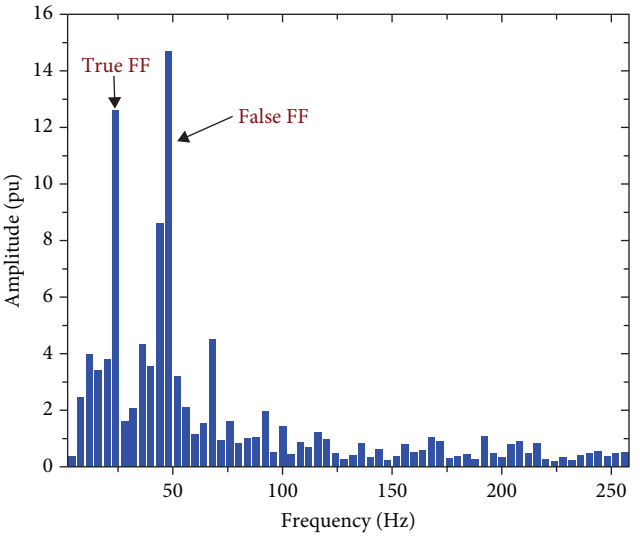

Figure 3: Spectrum of the contaminated vibration signal.

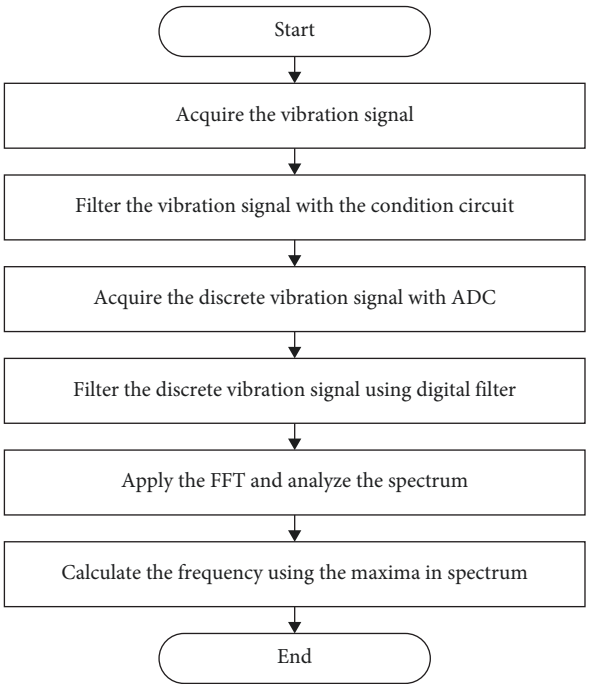

Figure 2: Flowchart of the frequency tracking based on vibration signal.

(5) Apply the FFT and search the maxima of the spectrum;

(6) Calculate the frequency using the maxima in the spectrum.

3. Materials and Methods

3.1. Problem Description. In this section, the problem of frequency tracking in practice is described using the scenario of an engine test of the automotive vehicle detection, which can be seen as the harshest working condition due to the vibration signal cannot be sampled directly from the engine due to high temperature and material of the engine, which makes the test suffer from various interferences, e.g., strong background noise, the vibration conduction from the test equipment. Under ideal conditions, the FF of the sampled vibration signal from the engine is obvious and easy to detect, as shown in Figure 1. However, the spectrum of practical vibration signals always suffers from the strong interferences produced by the sensor issues, vibration transmission, etc., leading to that the frequency cannot be accurately extracted from the collected vibration signal. Figure 3 gives one typical problematic spectrum in a practical vibration signal, and we can see that the true FF which should be the maxima has been overpassed by the false spectral line, which can produce wrong frequency estimations.

In Figure 4, the time–frequency analysis based on the wavelet transform of the vibration data sampled from a vehicle girder during the engine inspection is given. We can see that there are two main frequency curves, the lower one disconnects at the beginning of the test while the upper one, which is actually the true frequency, disconnects in the middle of the test, and this causes frequency-tracking error and the frequency-tracking errors with no doubt. To get more details, single frames of the spectrum corresponding to time A, B, and C in Figure 4 are given in Figure 5. It is seen that the true FF clearly shown in Figure 5(a) reduces to a very low level at Time B, and it becomes prominent again at Time C as shown in Figure 5(c). Meanwhile, the false one performs always prominently and continuously during the whole inspection. Thus, the main issues that could lead to wrong frequency-tracking results can be summarized based on the above analysis as follows:

(1) The energy of false FF overpasses the true one, as shown in Figure 3;

(2) The energy of the true FF weakens to a very low level, as shown in Figure 5(b);

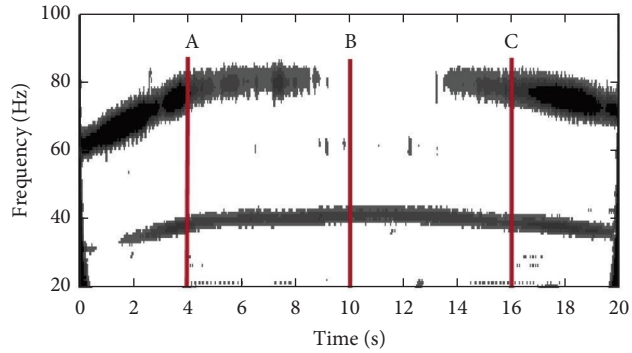

Figure 4: Time–frequency analysis of contaminated vibration signal based on wavelet.

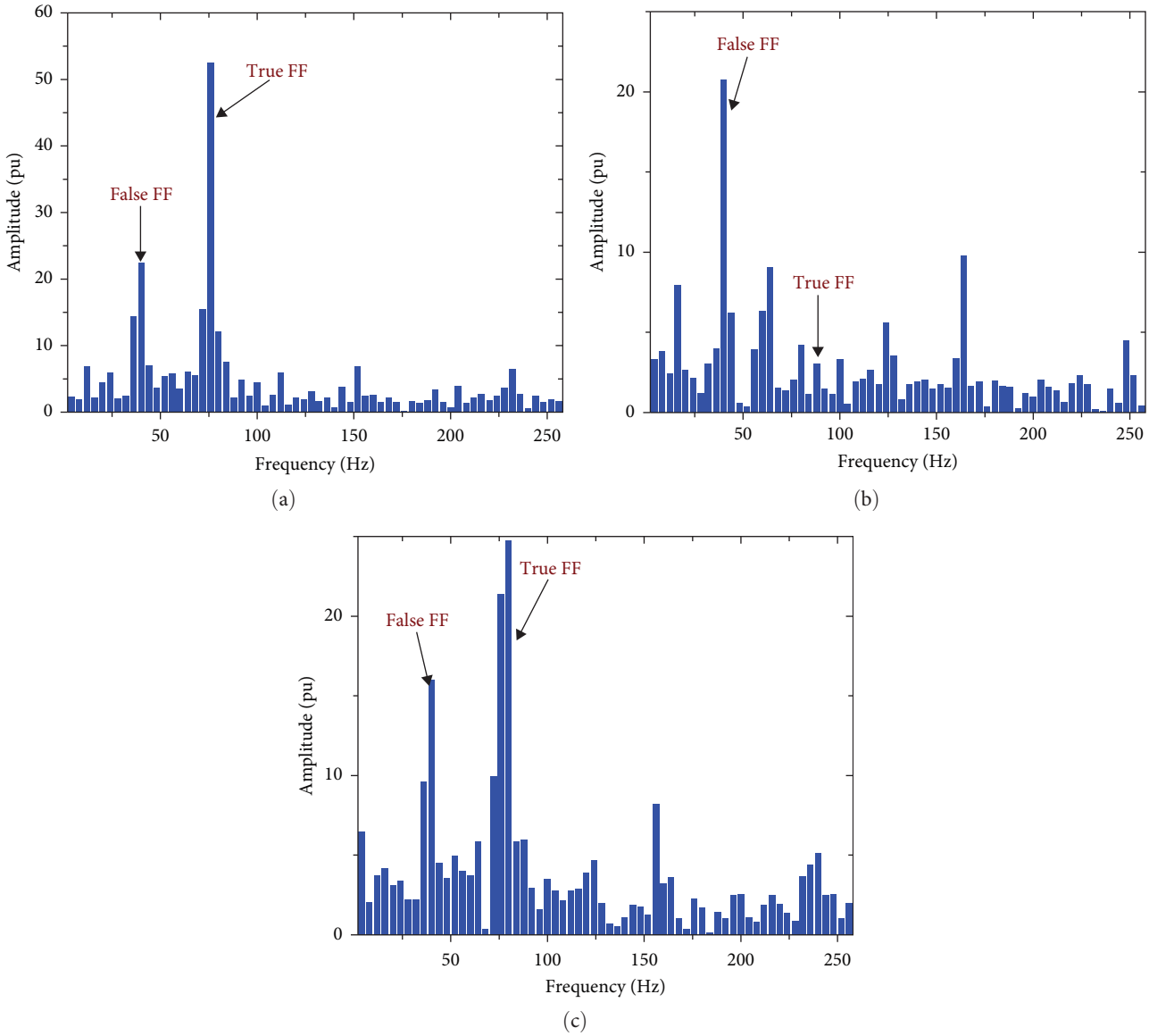

Figure 5: Comparison of the spectrum at different time: (a) Time A, (b) Time B, and (c) Time C.

Therefore, getting rid of the influence of the false component and locking the true frequency when it temporarily disappears is the key problem of the frequency-tracking task.

3.2. Frequency Tracking Using Cross-Correlation and KF. To solve the problems mentioned above in real-time frequency tracking, the cross-correlation and KF techniques are employed. The cross-correlation is based on the surface noise and vibration. Because the surface noise is sourced from the vibration, some similar features in the frequency domain can be found, and the surface noise is not easily disturbed by the construction of a rotating device, thereby the energy of true FF can be enhanced. KF is an outstanding tool for correcting the process noise from the measured signal, and it is adopted here to filter out the strong interfering component, i.e., the false FF, which surpassed the true one. With a suitable initial input value, there will be a statistically optimal state estimation produced by the KF.

3.2.1. Cross-Correlation. Define that the acquired surface noise is $s(n)$, which can be presented as follows:

$$s(n) = \sum_{l=1}^{L} [B_l(n) \sin(2\pi f_l(n) n + \delta_l(n))] + \zeta(n), \tag{4}$$

where $l = 1, 2, 3, \ldots, L$, L is the number of frequency components; B_l, f_l, and δ_l are the amplitude, frequency, and phase angle of, the l-th harmonic, respectively; ζ is the interference component of the surface noise signal. Comparing $s(n)$ with the vibration signal $x(n)$, under normal circumstances, some same frequency components exist due to their relationship. Then, the cross-correlation technique is applied to $s(n)$ with vibration signal $x(n)$ as follows:

$$R(n) = x(n) \times s(-n), \tag{5}$$

where $R(n)$ is the result of cross-correlation, and the length of $R(n)$ is fixed to $2N$ by zero-padding. Through this, the energy of the component with the same frequency can be enhanced.

3.2.2. Kalman Filter. The application of KF in real-time frequency tracking using the correlation coefficients of vibration and surface noise signal can be described generally by the following procedure.

First, define the state vector as follows:

$$\mathbf{x}_n = \begin{bmatrix} f_n \\ \Delta f_n \end{bmatrix}, \tag{6}$$

where the first element f_n of the vector is the average frequency during the time increment Δt, the second element Δf_n is the change rate of the frequency, and n represents the discrete time. Accordingly, the Δf_n is assumed to vary randomly in a small interval, which can be represented by a variable u_n following the Gaussian distribution.

Second, construct the difference process equation and measurement equation for real-time frequency tracking as follows:

$$f_n = f_{n-1} + \Delta f_{n-1} \cdot \Delta t + u_n \cdot \Delta t, \tag{7}$$

$$\Delta f_n = \Delta f_{n-1} + u_n, \tag{8}$$

$$y_n = f_n + v_n, \tag{9}$$

where y_n is the optimal frequency calculated by the KF at time n, and v_n represents a variable following the Gaussian distribution.

Finally, rewrite the difference process equation and measurement equation in matrix form as follows:

$$\mathbf{x}_n = \mathbf{A} f_{n-1} + \mathbf{e}_n, \tag{10}$$

$$y_n = \mathbf{H} f_n + v_n, \tag{11}$$

where

$$\mathbf{A} = \begin{bmatrix} 1 & \Delta t \\ 0 & 1 \end{bmatrix}, \quad \mathbf{G} = \begin{bmatrix} \Delta t \\ 1 \end{bmatrix}. \quad \mathbf{H} = [\,1 \quad 0\,], \quad \mathbf{e}_n = \mathbf{G} u_n \tag{12}$$

It should be noted that the above process is set up on the assumption that the noise $\mathbf{e}_n$ obeys the Gaussian distribution with zero mean value, and an initial input is needed as a priori for the measurement.

3.2.3. Interpolated Kalman Filter for Real-Time Frequency Tracking. With the adoption of the above technologies, for most of the scenarios, the true frequency can be found and tracked correctly in real time. However, in practice, under complex working conditions, the sampled data may be affected by even more strong interferences, resulting in difficulty in identifying and predicting the true frequency, and even the initial value is hard to obtain accurately, which can change the outcome totally.

To this end, an IKF is proposed for real-time frequency tracking in the practical conditions. The proposed IKF consists of three procedures, frequency search procedure (FSP), frequency lock procedure (FLP), and frequency correct procedure (FCP). In order to lower the computational burden, the KF is simplified to a one-dimension equation with a constant rate of change of the frequency as follows:

$$f_n = f_{n-1} + f_{\max} \cdot \Delta t, \tag{13}$$

where $f_{\max}$ is the frequency threshold larger than the frequency variation that can be produced by the device normally. Here, the bin number of spectral lines corresponding to the frequency is utilized in consideration of the computational burden, and an interpolated FFT is adopted to restrain the spectrum leakage and increase the accuracy level of frequency estimation. The details of the three mentioned steps are described as follows:

(1) The aim of FSP is to find the proper bin number corresponding to the FF from the spectrum of the

cross-correlation coefficients of vibration and surface noise signals. Here, a vector including four optional bin numbers is selected to be the input of the step which is presented as follows:

$$\mathbf{x}_{n-1} = [\, k1_{n-1} \quad k2_{n-1} \quad k3_{n-1} \quad k4_{n-1} \quad \Delta k \,]^{\mathrm{T}}, \tag{14}$$

where $k1$, $k2$, $k3$, and $k4$ represent the positions of the first four extremes with the largest amplitude in the spectrum of the cross-correlation coefficients, Δk means the positon variation corresponding to the max rate of change of frequency.

By ignoring the effect of process error and measurement error, Equations (10) and (11) are rewritten as follows:

$$\mathbf{X}_n = \lceil \mathbf{A}\mathbf{X}_{n-1} \rceil, \tag{15}$$

where the symbol "⌈⌉" means operation of rounding up to an integer, and the matrix $\mathbf{A}$ is presented as follows:

$$\mathbf{A} = \begin{bmatrix} 1 & 0 & 0 & 0 & \Delta t \\ 1 & 0 & 0 & 0 & \Delta t \\ 1 & 0 & 0 & 0 & \Delta t \\ 1 & 0 & 0 & 0 & \Delta t \\ 0 & 0 & 0 & 0 & 1 \end{bmatrix}. \tag{16}$$

Accordingly, four proper alternative frequency components are tracked by the KF, thereafter one proper frequency is chosen by comparing the continuity and stability of the spectrum amplitudes of four frequency values and the ratio between the options according to the characteristics of the device to be tested.

(2) FLP is used to eliminate the interferences and carry out the right frequency after FSP. Once the main frequency obtained from FSP is confirmed, it will be selected as the input of FLP. Here, the function which takes the measurement error into account is transformed as follows:

$$k_n = k_{n-1} + k_{\max} \cdot \Delta t, \tag{17}$$

where k_{n-1} is the input given by FSP, and $k_{\max}$ is the max change of spectral position corresponding to $f_{\max}$.

In order to improve the accuracy level of frequency estimation using fewer samples, as fewer samples, mean lower computational burden and higher time resolution, a double-spectrum-line interpolation procedure based on a N-point trapezoid self-convolution window (TSCW) is applied. The TSCW, which has better interference suppression is used to truncate the vibration sequence as follows:

$$z(n) = x(n) \cdot w_{\mathrm{Tra}-p}(n), \tag{18}$$

where the expression of TSCW is given as follows:

$$w_{\mathrm{Tra}-p}(n) = \underbrace{w_{\mathrm{Tra}}(m) \times w_{\mathrm{Tra}}(m) \times \cdots \times w_{\mathrm{Tra}}(m)}_{p}, \tag{19}$$

where p is the order of TSCW, $w_{\mathrm{Tra}}(m)$ is the discrete time domain function of the trapezoid window, $m = 0, 1, \ldots, M-1$, the p-th-order TSCW is padded with $p-1$ zeros in order to achieve a sequence of length $L = pM$. With TSCW, the frequency estimation can be acquired by:

$$f = (k_{\mathrm{m}} + \alpha) \cdot f_{\mathrm{s}}/N, \tag{20}$$

where α is the calibration coefficient calculated by:

$$\begin{cases} \alpha = \mathbf{C}\mathbf{Q} \\ \mathbf{C} = [\, c_1 \quad c_3 \quad c_5 \quad c_7 \,], \\ \mathbf{Q} = [\, \beta \quad \beta^3 \quad \beta^5 \quad \beta^7 \,]^{\mathrm{T}} \end{cases} \tag{21}$$

where $\mathbf{C}$ is the coefficient vector whose values are 0.1154, 0.1817, 0.3414, and 4.735, respectively, and β is a value calculated as follows:

$$\beta = \frac{k_{\mathrm{m}} - k_{\mathrm{s}}}{k_{\mathrm{m}} + k_{\mathrm{s}}}, \tag{22}$$

where k_{m} is the bin number of maxima in the range $[k_n/2-1,\ k_n/2+1]$ of the spectrum of the N-point vibration signal, while k_{s} is the position of the larger one of the adjacent lines to k_{m}. It should be noted that the surface noise is used only to determine the position of the FF, while the refining of the estimation still depends on the vibration signal.

(3) FCP is used to monitor the frequency-tracking process and correct the frequency when bugs occur. In practice, it is inevitable that bugs occur in frequency tracking because of the diversity of measurements, e.g., the wrong frequency is occasionally obtained from FSP, if the wrong frequency component lasts for a while, the FLP may lock this wrong frequency component. To solve this problem, FCP based on amplitude comparison is needed. The mechanism can be described as the continuous count of the number of inconsistencies between the amplitude of the locked frequency and the maximum value of the spectrum will be recorded to determine whether the locked frequency is wrong. The amplitude difference is calculated as follows:

$$T = A_{\max} - A_f, \tag{23}$$

where A_f is the magnitude of the spectral line k_{m}, and $A_{\max}$ is the maxima of the spectrum of the vibration

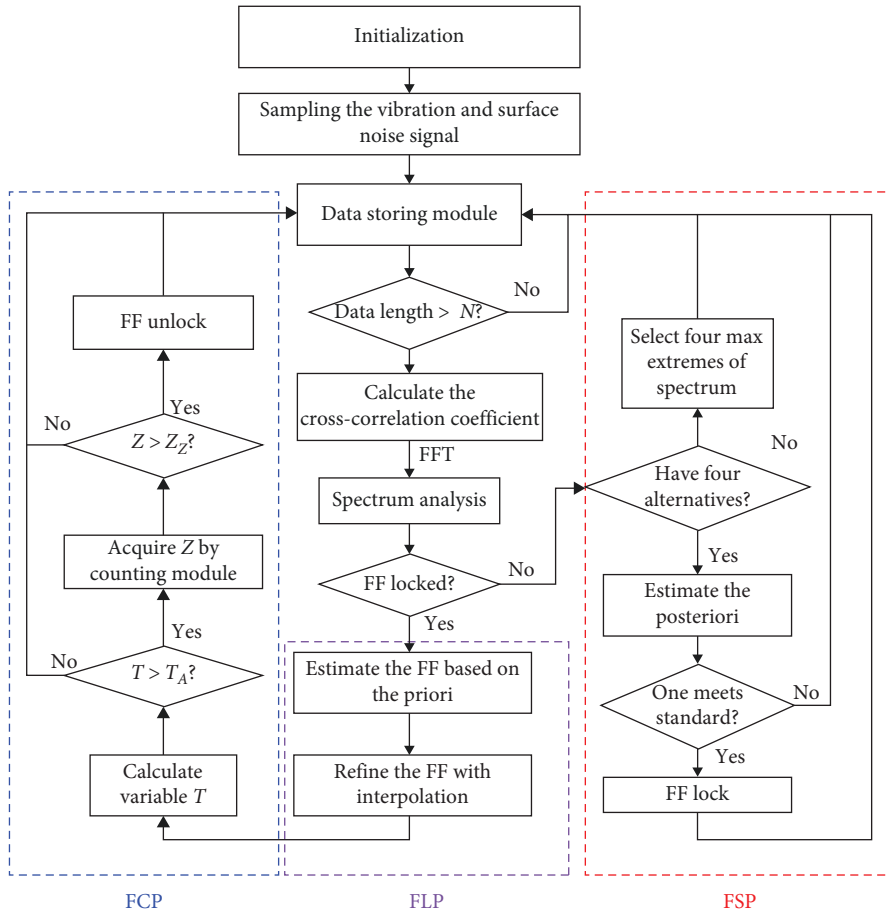

Figure 6: Flowchart of frequency-tracking method based on cross-correlation and KF.

signal. Here are two thresholds, i.e., T_A and T_z, are given and adopted to give assistance. T_A is related to the amplitude difference, while T_z represents a time-related threshold for the count limit. T_A is always set to 10% of the maxima in the spectrum according to the practical tests, i.e., if $T > T_A = 0.1A_{\max}$, it can be considered that there is an anomaly in the frequency-tracking task, then the variable Z of the counting module will plus 1; otherwise, Z will be reset to 0. T_z here is determined by the sampling frequency, the measurement gap, and the requirement of specific applications.

The flowchart of the proposed IKF can be described in Figure 6.

4. Results and Discussion

In order to evaluate the performance of the proposed method in real-time frequency tracking, an ARM-based test bench which can acquire the raw vibration and surface noise signals and process the sampled data through different methods to estimate the frequency, is set up. The working flow of the test bench can be stated as the vibration and noise sensors attached to a magnetic material are first absorbed by the tested device directly, and the raw signals are synchronously transferred through the coaxial cable to avoid unwanted

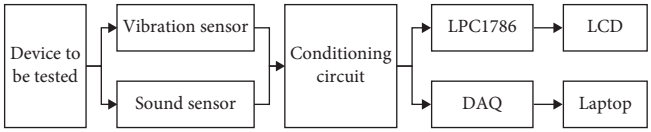

Figure 7: Diagram of the test bench setup.

transmission noise. Second, the analog signals filtered by the conditioning circuit are sampled through the internal ADC of the processor LPC1768. Then, the conditioned raw data are processed digitally for storing, filtering, and analyzing. At last, the frequency-tracking result will be displayed on the LCD. For the sake of convenience, the raw signals are captured by a laptop simultaneously by a DAQ unit. The schematic of the test bench setup is shown in Figure 7.

The implemented test signals include the standard vibration signal produced by the standard vibration exciter and the other two kinds of vibration signals sampled from the shaft of a diesel vehicle engine. The test bench consists of the ARM processor LPC1768@100MHz, the acceleration sensor MMA1220KEG, and a thin-film-Mic-based LM386 noise acquisition module. To make comparisons, FFT without filter, FFT with normal KF, and the SDFT [33] are employed in considerations of the limited performance of the test bench. In addition, the WT-based frequency estimator is executed

Figure 8: Setup of the test bench for standard vibration signal measurement.

Table 1: Frequency measurement accuracy of signals generated by the standard vibration exciter (Hz).

Frequency	FFT	KF	WT	SDFT	IKF	Frequency	FFT	KF	WT	SDFT	IKF
20	0	0	1.0E-1	1.0E-3	1.5E-3	20.2	0.2	0.2	8.0E-3	1.1E-3	2.3E-3
30	0	0	8.6E-2	3.2E-3	3.1E-3	30.3	0.3	0.3	1.7E-2	3.3E-3	4.4E-3
40	0	0	2.5E-1	2.9E-3	6.4E-3	40.7	0.7	0.7	3.7E-2	4.8E-3	7.2E-3
50	0	0	7.1E-2	6.7E-3	7.3E-3	52.3	0.3	0.3	6.5E-1	6.1E-3	7.9E-3
60	0	0	3.1E-1	8.3E-3	8.1E-3	61.3	0.7	1.3	4.6E-2	8.8E-3	9.2E-3
75	1	1	9.4E-2	7.9E-3	8.8E-3	75.3	0.7	1.3	2.2E-1	8.9E-3	9.9E-3
80	0	0	4.4E-1	7.1E-3	8.9E-3	80.3	0.3	0.3	7.0E-1	1.0E-3	1.1E-2
97	1	1	5.2E-1	8.8E-3	9.8E-3	97.7	0.3	1.7	8.3E-2	9.9E-3	1.1E-2
100	0	0	4.9E-1	9.6E-3	9.5E-3	102.7	0.7	0.7	5.3E-1	1.2E-2	1.2E-2
120	0	0	6.9E-1	9.9E-3	9.9E-3	122.3	0.3	0.3	7.5E-2	1.2E-2	1.2E-2

on the laptop because of the computational complexity. The sampling frequency f_s is set to 512 Hz, since the main frequency of the engine under test is below 200 Hz. The FFT length N in IKF, i3DFT, and SDFT is set to 128 to acquire more details of the frequency variation, while the length of FFT without filter and FFT with normal KF is 256 to enhance the frequency resolution. Besides, the measurement gap D is fixed to 10 to supply a proper time resolution. According to the requirement of the engine test, T_z is set to 20, corresponding to 400 ms approximately. The order of TSCW adopted in IKF is 4.

4.1. Measurement of Standard Signal. The standard vibration and surface noise signals of different frequency values are generated by a platform consisting of a power amplifier YMC LA-100 and a standard vibration exciter YMC VT-150, then sampled and processed by the test bench, which is shown in Figure 8. The absolute errors of frequency measured by different methods are tabulated in Table 1, where the results with a dark background indicate the minimum values among the adopted methods under the same test condition.

According to the results given in Table 1, compared to the traditional methods like FFT and WT, it can be known that the IKF performs excellently in the measurement range. The results of SDFT show the best on most of the test frequency points. The reason can be interpreted as, the SDFT has outstanding anti-noise ability while the superiority of the windowed interpolation FFT adopted in IKF is the harmonic suppression, and the main interference in this measurement is the noise. Fortunately, the accuracy level of IKF can meet the requirement of the frequency tracking for the RPM test, and a better frequency estimator can be adopted in FLP if necessary. Although, the results of FFT and KF listed on the left side represent 0 absolute error on some integer test points due to the synchronous sampling, their errors increase dramatically when it is under asynchronous sampling, which cannot meet the requirement of some applications with high-accuracy measurement. For the WT, it suffers from the high computational burden, and this may make it not the best choice for real-time frequency tracking with the limited computing power.

4.2. Frequency Tracking for a Signal with an Obvious FF. Here, the vibration and noise signals are sampled in a vehicle inspection and test station from the shaft of a nearly new

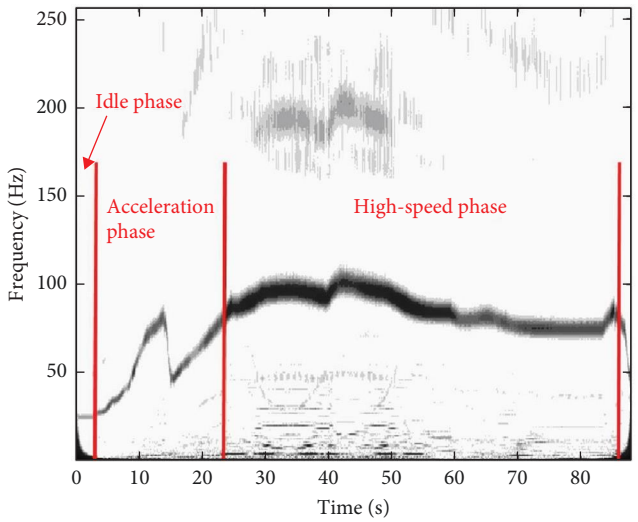

Figure 9: Time–frequency analysis of the test signal with an obvious FF.

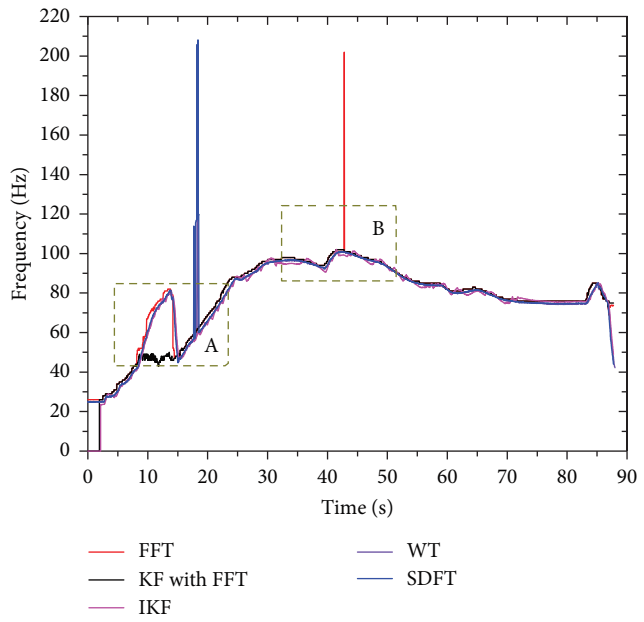

Figure 10: The result of frequency tracking of the obvious FF signal.

vehicle whose engine and other parts are well working. The time–frequency analysis of the vibration signal based on the wavelet transform is shown in Figure 9.

In Figure 9, the darker the color, the stronger the energy, and we can see that the frequency curve of the sampled signal is clearly described by the background. From Figure 9, it can be known that the engine testing is mainly divided into three stages, i.e., idle phase, acceleration phase, and high-speed phase. In the idle phase, the frequency keeps in the low range steadily, in the acceleration phase, the frequency rises and falls rapidly, and in the high-speed phase, the frequency keeps in the higher range with slow change. Figure 10 demonstrates the analysis result of frequency tracked by FFT, KF, WT, SDFT, and IKF.

Based on Figure 10, it is known that the frequency change of the signal, as well as details of the variations, are tracked clearly and accurately through IKF. Although the other four methods could also track the frequency when detecting the engine, there still exist some places where the wrong result occurred, and this phenomenon is undesired in the practical detection. The errors that occurred in Figure 10, i.e., Place A where the KF locked the wrong spectral line, WT and SDFT suffered from the strong components, and Place B where the FFT emerged as an error, are enlarged in Figure 11.

Figure 11(a) is the detail of the acceleration phase where the Box A shows. From Figure 11(a), we can see that the FFT, WT, SDFT, and IKF could estimate the frequency variations correctly while the KF caught an error. Then, WT and SDFT suffered from strong harmonics, which produced large frequency errors. Furthermore, the IKF estimates the frequency smoothly while the FFT and WT still fluctuate in some test points. The reason can be interpreted as that the KF is vulnerable to being affected by a continuous frequency component, which may lead to a series of measurement mistakes. Figure 11(b) is the enlarged detail of Box B which is in the high-speed phase. It is seen that the adopted methods could give a ballpark estimation of the frequency except the FFT which estimates the frequency wrongly for a very short duration with large hopping points. That means, although the FFT is simple, it lacks the immunity to the unavoidable error that may occur during the practical test.

In conclusion, the performance of the adopted five methods is eligible in most of the time when the frequency component of the sampled signal is obvious. Unfortunately, FFT WT, KF, and SDFT still cannot meet the requirement of the frequency tracking in the scenario of a practical test because of the unacceptable error that occurred in the measurement. Another point that needs to be mentioned is that, even in an ideal test environment, there will be unexpected interference.

4.3. Frequency Tracking for a Signal with Multifrequency. Similarly, the signal is sampled in a vehicle inspection and test station and it is acquired from the shaft of a truck that has been in use for more than 6 years. The time–frequency analysis based on the wavelet transform of the sampled vibration and surface noise signals is shown in Figure 12.

According to Figure 12(a), it can be seen that, at the beginning of the test, there are three main frequency components, the FF, and two harmonics, and the consecutiveness of these components is quite excellent. Subsequently, the harmonics become weak and ambiguous, while the fundamental one becomes stronger and maintains the status until the end. Correspondingly, we can see that, in Figure 12(b), similar features can be found in the time–frequency analysis of the surface noise, whereas the energy level is much lower than the vibration. It should be highlighted that a subharmonic appears during the frequency ascent stage which could affect the measurement. The results of frequency tracking by FFT, KF, and IKF are represented in Figure 13.

From Figure 13, we can see that the proposed method can track the frequency accurately during the whole test. The KF tracked the wrong frequency component from the

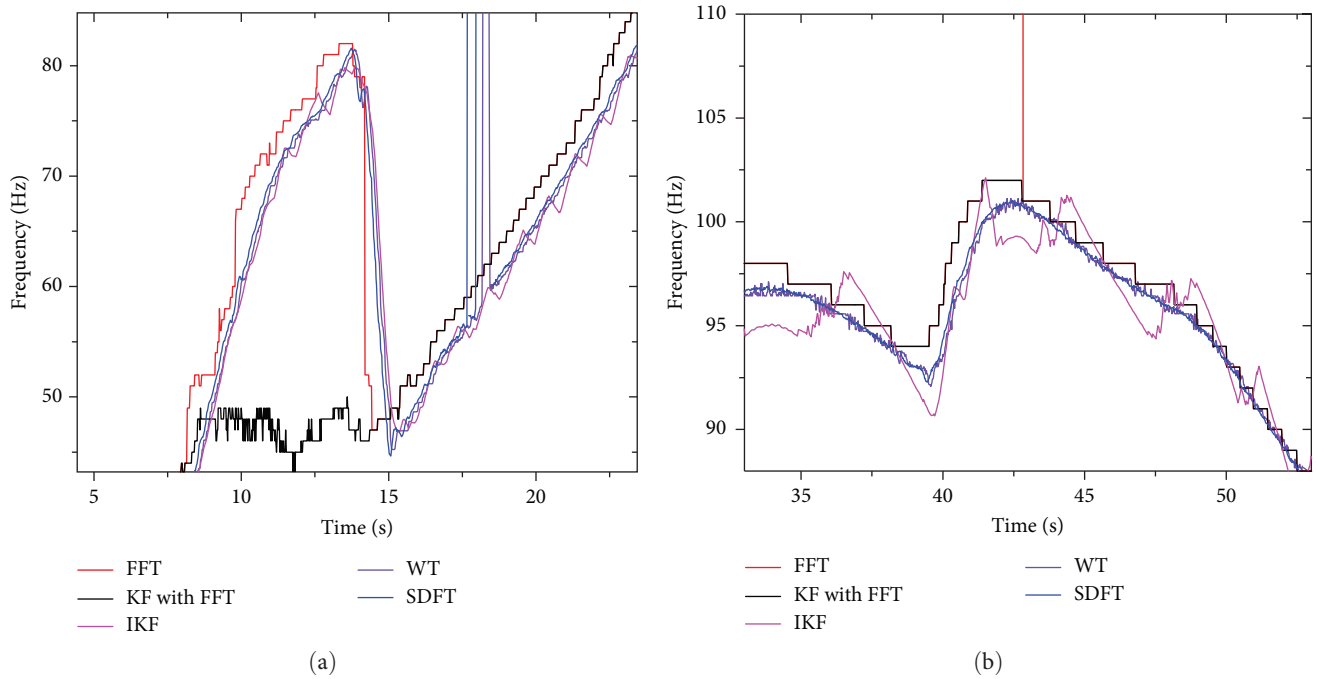

Figure 11: Partially enlarged detail in Figure 10: (a) Box A and (b) Box B.

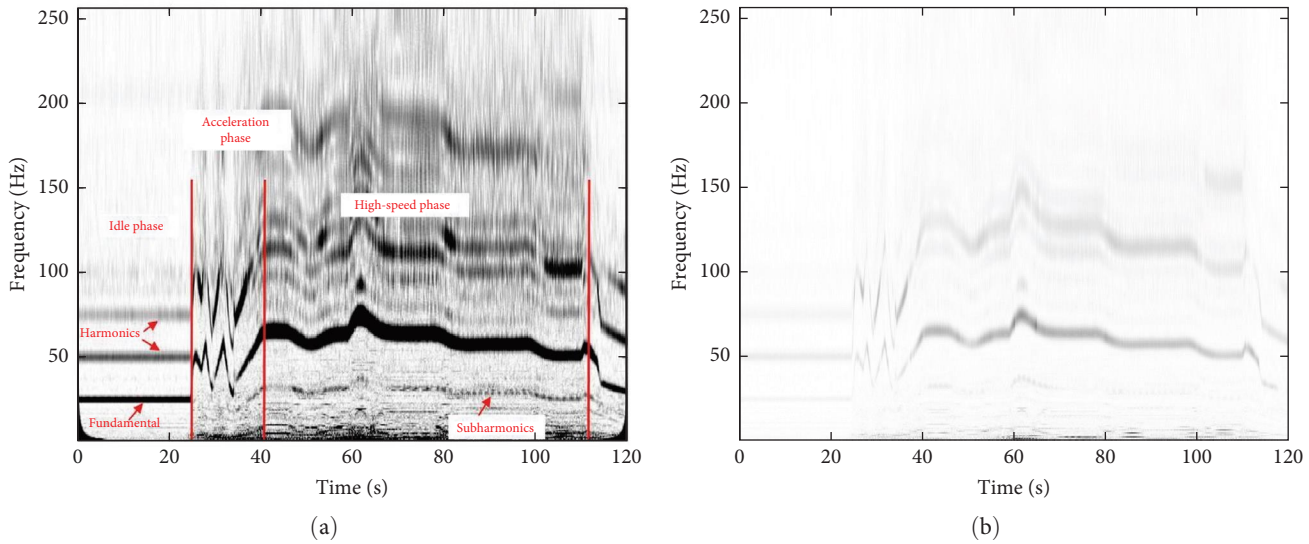

Figure 12: Time–frequency analysis of the sampled multifrequency signal: (a) vibration signal and (b) surface noise signal.

beginning, while the FFT can track the frequency in the high-frequency range. However, the FFT failed to estimate the correct frequency in the phase of rapid frequency change. Focus on the curves in the dashed box, we can see that the results of FFT, WT, and SDFT varied fiercely while the KF was trapped in a wrong frequency component. Fortunately, thanks to the domain position of the main component in the high-frequency range, FFT, WT, and SDFT returned to the right result, while KF tracked to the wrong component during the whole test even with an outstanding FF component in the high-frequency range because of the lack of the correction module.

The reason can be described as that, on account of strong interferences, e.g., high energy background noise, all kinds of harmonics whose intensity exceeds the fundamental wave, etc., the spectrum became complex, making the FFT, WT, and SDFT alternate between the right and the wrong spectral lines, which resulted that the measurement result turned to be chaotic. As for the KF, it encountered the same problem that occurred in subsection 4.2. The reason is similarly described

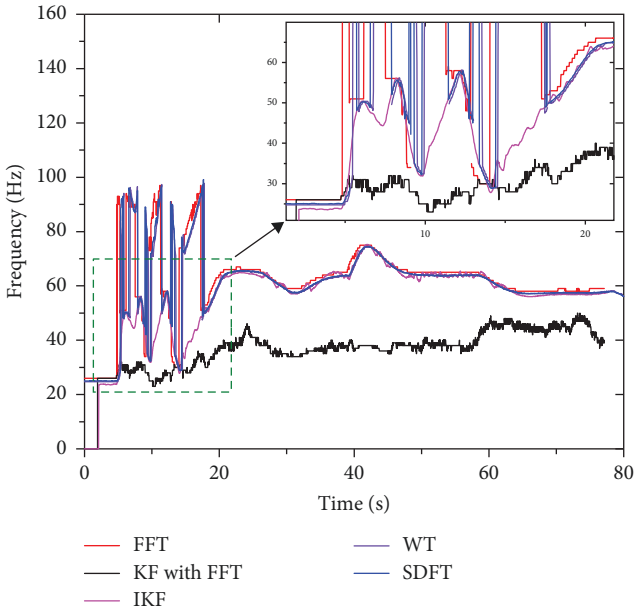

Figure 13: The result of frequency tracking of the sampled multifrequency signal.

as the KF is easily affected by the complex interferences if the surface noise and the correction module are lacking.

Based on the utilization results shown in Figures 10 and 13, it can be seen that the frequency of the given signals calculated by IKF is tremendously keeping pace with the variations of the simulated signal which shows the accuracy of the proposed method, which means the proposed method can solve the issue in practical real-time frequency tracking perfectly.

5. Conclusions

As one of the most important indicators of the condition monitoring and fault diagnosis of the rotating machinery, frequency tracking suffers from various interferences in the practical tests. In this paper, an IKF using cross-correlation of the vibration and surface noise signals is proposed to track the frequency variations. In order to enhance the energy concentration of the FF, the cross-correlation technique is employed by convolution of the synchronized sampled surface vibration and noise signals. Meanwhile, the two-point interpolated FFT based on TSCW is adopted to improve the measurement accuracy and reduce the computational burden. To evaluate the proposed method, an ARM-based embedded test bench is set to acquire the surface vibration and noise signals and then execute the proposed method to estimate frequency in real time. According to the results, it is known that the proposed method can improve the frequency-tracking accuracy and perform perfectly under simple or complex working conditions.

Data Availability

Data for this research article are available upon request to the authors.

Conflicts of Interest

The authors declare that there is no conflict of interest regarding the publication of this paper.

References

[1] X. Wang, U. Kruger, G. W. Irwin, G. McCullough, and N. McDowell, "Nonlinear PCA with the local approach for diesel engine fault detection and diagnosis," *IEEE Transactions on Control Systems Technology*, vol. 16, no. 1, pp. 122–129, 2008.

[2] R. Wang, H. Chen, and C. Guan, "DPGCN model: a novel fault diagnosis method for marine diesel engines based on imbalanced datasets," *IEEE Transactions on Instrumentation and Measurement*, vol. 72, pp. 1–11, 2023.

[3] A. Mehta, D. Goyal, A. Choudhary, B. S. Pabla, and S. Belghith, "Machine learning-based fault diagnosis of self-aligning bearings for rotating machinery using infrared thermography," *Mathematical Problems in Engineering*, vol. 2021, Article ID 9947300, 15 pages, 2021.

[4] L. Dong, J. Jatskevich, Y. Huang, M. Chapariha, and J. Liu, "Fault diagnosis and signal reconstruction of hall sensors in brushless permanent magnet motor drives," *IEEE Transactions on Energy Conversion*, vol. 31, no. 1, pp. 118–131, 2016.

[5] A. Usman and B. S. Rajpurohit, "Time-efficient fault diagnosis of a BLDC motor drive deployed in electric vehicle applications," in *2020 IEEE Global Humanitarian Technology Conference (GHTC)*, pp. 1–5, IEEE, Seattle, WA, USA, 2020.

[6] A. Brandt, *Noise and Vibration Analysis: Signal Analysis and Experimental Procedures*, John Wiley & Sons, 2023.

[7] X. Chen and Z. Feng, "Order spectrum analysis enhanced by surrogate test and Vold–Kalman filtering for rotating machinery fault diagnosis under time-varying speed conditions," *Mechanical Systems and Signal Processing*, vol. 154, Article ID 107585, 2021.

[8] X. He, Q. Zhang, J. Ding, and W. Zhao, "Wheelset-bearing fault feature extraction from multi-impulsive signals under time-varying speed conditions," *IEEE Transactions on Instrumentation and Measurement*, vol. 72, pp. 1–12, 2023.

[9] S. Lu, R. Yan, Y. Liu, and Q. Wang, "Tacholess speed estimation in order tracking: a review with application to rotating machine fault diagnosis," *IEEE Transactions on Instrumentation and Measurement*, vol. 68, no. 7, pp. 2315–2332, 2019.

[10] H. Li, X. Wu, T. Liu, and S. Li, "Rotating machinery fault diagnosis based on typical resonance demodulation methods: a review," *IEEE Sensors Journal*, vol. 23, no. 7, pp. 6439–6459, 2023.

[11] B. Peng, S. Wan, Y. Bi, B. Xue, and M. Zhang, "Automatic feature extraction and construction using genetic programming for rotating machinery fault diagnosis," *IEEE Transactions on Cybernetics*, vol. 51, no. 10, pp. 4909–4923, 2021.

[12] F. Wang, L. Wang, Y. Wen, F. Ha, J. Lu, and W. Jiao, "Intelligent diesel engine fault diagnosis method based on time–frequency-nonconvex robust principal component analysis," in *2022 International Conference on Sensing, Measurement & Data Analytics in the Era of Artificial Intelligence (ICSMD)*, pp. 1–5, IEEE, Harbin, China, 2022.

[13] Y. Li, B. Tang, X. Jiang, and Y. Yi, "Bearing fault feature extraction method based on GA-VMD and center frequency," *Mathematical Problems in Engineering*, vol. 2022, Article ID 2058258, 19 pages, 2022.

[14] C. Zhang, B. Chen, F. Wan, and B. Song, "Multi-faults diagnosis of rotating bearings using flexible time–frequency analysis technique," in *2018 International Conference on Sensing, Diagnostics, Prognostics, and Control (SDPC)*, pp. 347–352, IEEE, Xi'an, China, August 2018.

[15] S. Huang, K. K. Tan, and T. H. Lee, "Fault diagnosis and fault-tolerant control in linear drives using the Kalman filter," *IEEE Transactions on Industrial Electronics*, vol. 59, no. 11, pp. 4285–4292, 2012.

[16] H. Toshani, S. Abdi, N. K. Hosseini, and E. Abdi, "Fault diagnosis of squirrel cage induction generator for wind turbine applications using a hybrid deep neural network and decision tree approach," in *2021 International Conference on Electrical, Computer and Energy Technologies (ICECET)*, pp. 1–6, IEEE, Cape Town, South Africa, December 2021.

[17] H. Li, C. Sun, L. Lu, and H. Wang, "Research on fault diagnosis of ship generator based on GA-BP neural network," in *2022 7th International Conference on Automation, Control and Robotics Engineering (CACRE)*, pp. 234–238, IEEE, Xi'an, China, July 2022.

[18] D. Zhang and Z. Feng, "Enhancement of time–frequency post-processing readability for nonstationary signal analysis of rotating machinery: principle and validation," *Mechanical Systems and Signal Processing*, vol. 163, Article ID 108145, 2022.

[19] M. Tiboni, C. Remino, R. Bussola, and C. Amici, "A review on vibration-based condition monitoring of rotating machinery," *Applied Sciences*, vol. 12, no. 3, Article ID 972, 2022.

[20] M. Kunli and W. Yunxin, "Fault diagnosis of rolling element bearing based on vibration frequency analysis," in *2011 Third International Conference on Measuring Technology and Mechatronics Automation*, vol. 2, pp. 198–201, IEEE, Shanghai, China, January 2011.

[21] G. Toh and J. Park, "Review of vibration-based structural health monitoring using deep learning," *Applied Sciences*, vol. 10, no. 5, Article ID 1680, 2020.

[22] Z. Wang, J. Yang, and Y. Guo, "Unknown fault feature extraction of rolling bearings under variable speed conditions based on statistical complexity measures," *Mechanical Systems and Signal Processing*, vol. 172, Article ID 108964, 2022.

[23] Y. Yin, Z. Liu, M. Zuo, Z. Zhou, and J. Zhang, "A three-dimensional vibration data compression method for rolling bearing condition monitoring," *IEEE Transactions on Instrumentation and Measurement*, vol. 72, pp. 1–10, 2023.

[24] Z. Xu, J. Wang, and Y. Shen, "Weak faults diagnosis for rolling bearings based on variational Hilbert Huang transform," in *2020 11th International Conference on Prognostics and System Health Management (PHM-2020 Jinan)*, pp. 471–476, IEEE, Jinan, China, October 2020.

[25] S. Nima Mahmoodi, M. J. Craft, S. C. Southward, and M. Ahmadian, "Active vibration control using optimized modified acceleration feedback with adaptive line enhancer for frequency tracking," *Journal of Sound and Vibration*, vol. 330, no. 7, pp. 1300–1311, 2011.

[26] L. Song, H. Wang, and P. Chen, "Vibration-based intelligent fault diagnosis for roller bearings in low-speed rotating machinery," *IEEE Transactions on Instrumentation and Measurement*, vol. 67, no. 8, pp. 1887–1899, 2018.

[27] C. Wang, X. Liu, and Z. Chen, "Incipient stator insulation fault detection of permanent magnet synchronous wind generators based on HILBERT–Huang transformation," *IEEE Transactions on Magnetics*, vol. 50, no. 11, pp. 1–4, 2014.

[28] Z. Wu and N. E. Huang, "Ensemble empirical mode decomposition: a noise-assisted data analysis method," *Advances in Adaptive Data Analysis*, vol. 1, no. 1, pp. 1–41, 2009.

[29] D. Tang, F. Bi, J. Lin, X. Li, X. Yang, and X. Bi, "Adaptive recursive variational mode decomposition for multiple engine faults detection," *IEEE Transactions on Instrumentation and Measurement*, vol. 71, pp. 1–11, 2022.

[30] A. Taghizadeh-Alisaraei and A. Mahdavian, "Fault detection of injectors in diesel engines using vibration time–frequency analysis," *Applied Acoustics*, vol. 143, pp. 48–58, 2019.

[31] H. Wen, J. Zhang, Z. Meng, S. Guo, F. Li, and Y. Yang, "Harmonic estimation using symmetrical interpolation FFT based on triangular self-convolution window," *IEEE Transactions on Industrial Informatics*, vol. 11, no. 1, pp. 16–26, 2015.

[32] J. Song, J. Zhang, A. Mingotti, L. Peretto, and H. Wen, "Novel two-point interpolation DFT method for frequency estimation of sine-wave within a short time window," in *2022 IEEE 12th International Workshop on Applied Measurements for Power Systems (AMPS)*, pp. 1–6, IEEE, Cagliari, Italy, September 2022.

[33] Y. Sun, C. Zhuang, and Z. Xiong, "A scale factor-based interpolated DFT for chatter frequency estimation," *IEEE Transactions on Instrumentation and Measurement*, vol. 64, no. 10, pp. 2666–2678, 2015.

[34] M. S. Qatu, M. K. Abdelhamid, J. Pang, and G. Sheng, "Overview of automotive noise and vibration," *International Journal of Vehicle Noise and Vibration*, vol. 5, no. 1/2, pp. 1–35, 2009.

[35] J. Tuma, "Gearbox noise and vibration prediction and control," *International Journal of Acoustics and Vibration*, vol. 14, no. 2, pp. 99–108, 2009.

[36] H. Jingzhu, L. Dichen, L. Qingfen, Y. Yang, and L. Shanshan, "Electromagnetic vibration noise analysis of transformer windings and core," *IET Electric Power Applications*, vol. 10, no. 4, pp. 251–257, 2016.

[37] J. Černetič, "The use of noise and vibration signals for detecting cavitation in kinetic pumps," *Proceedings of the Institution of Mechanical Engineers, Part C: Journal of Mechanical Engineering Science*, vol. 223, no. 7, pp. 1645–1655, 2009.